Temperature-Dependent Spin Relaxation: A Major Factor in Electron Backward Transfer Following the Quenching of *$Ru(bpy)_3^{2+}$ by Methyl Viologen†

Karsten A. Hötzer, Andreas Klingert, Thomas Klumpp, Evgenii Krissinel,‡ Dieter Bürssner, and Ulrich E. Steiner*

Fachbereich Chemie, Universität Konstanz, 78457 Konstanz, Germany

The magnetic-field dependence of the cage escape efficiency (φ_{ce}) of $[Ru(bpy)_3]^{3+}$ and methyl viologen radicals ($MV^{+\bullet}$) from the primary redox pair formed upon quenching of photoexcited $[Ru(bpy)_3]^{2+}$ by MV^{2+} was measured by laser flash spectroscopy in aqueous solution as a function of the magnetic field (0−2.85 T) in the temperature range from 5 to 69 °C. Furthermore, the ^{1}H NMR T_1 times of the paramagnetic $[Ru(bpy)_3]^{3+}$ were measured between −40 and 42 °C. The kinetic data were analyzed in terms of a kinetic model that takes into account spin conservation in the forward reaction between the ^{3}MLCT state of $[Ru(bpy)_3]^{2+}$ and the electron acceptor MV^{2+} yielding a triplet spin-correlated radical pair (RP) and the in-cage backward electron transfer requiring singlet character of the RP. The triplet-to-singlet spin conversion of the geminate RP is explicitly treated by the stochastic Liouville equation formalism. By theoretical simulation of the observed magnetic field dependence of φ_{ce}, the temperature dependent absolute values of the rate constants k_{ce} (cage escape), k_{bet} (backward electron transfer in singlet RPs), and k_{TS} (magnetic-field independent triplet-to-singlet interconversion) could be assessed. The temperature dependence of k_{ce} exhibits a very good proportionality to the solvent viscosity. The values obtained for k_{TS} are in good agreement with the results on the electron spin relaxation time of $[Ru(bpy)_3]^{3+}$ derived by the Solomon relation from the ^{1}H NMR T_1 times. The effective rate of backward electron transfer in the geminate RP turns out to be close to spin-controlled, i.e., it is determined by the rate constant k_{TS} of the triplet−singlet spin conversion process. The true rate constant k_{bet}, varying from 5.5×10^{10} s^{-1} to 1.2×10^{11} s^{-1}, is about seven times larger than the effective value for the total backward electron transfer comprising spin conversion and spin-allowed backward electron transfer.

1. Introduction

During the past 35 years an area of research has been established that connects the field of reaction kinetics and mechanisms with the field of magnetic resonance spectroscopy. This branch of physical chemical science, spin chemistry, deals with the role and effects of paramagnetic reaction intermediates occurring in pairs, most prominently radical pairs, or as molecular triplet states. The effects observed are non-Boltzmann polarizations of nuclei (CIDNP) and electrons (CIDEP) and/or magnetic field effects (MFEs) on rates and yields of chemical reactions. The relevance of such phenomena to reaction kinetics is due to the fact that spin processes, usually involving nearly degenerate sets of spin levels, which is the reason Zeeman splittings much smaller than thermal energies may have appreciable effects, are kinetically coupled to spin-selective chemical processes. Thus the spin chemical effects can be exploited as diagnostic tools not only of the spin processes themselves but of the whole reaction mechanism of which they are a part. For selected reviews, see refs 1−6.

It is of importance to note that the time scale of reactions that can be probed by spin chemistry is defined by the time-scale of spin processes that lead to multiplicity changes, e.g., in a radical pair (RP). Here one has to distinguish between coherent spin processes that are due to interactions such as isotropic hyperfine coupling and Zeeman interaction, notably the difference between the two radicals in a pair, and incoherent spin processes, usually described as spin relaxation, that is due to fluctuating magnetic fields. The typical time scale for these processes in organic RPs is nanoseconds to microseconds. Much shorter time scales, however, apply to many paramagnetic transition metal complexes. Here paramagnetic relaxation times on the picosecond time scale can be found[7] that may be assigned to the effect of collisional modulation of spin−orbit coupling (SOC). The effects of strong SOC appear also in large anisotropy and large deviations of the *g*-factor from the value of the free electron, which is essentially found in typical organic radicals. Thus, in strong magnetic fields of several Tesla, the difference in Larmor precession time periods of a paramagnetic transition metal complex and an organic counter radical may even be pushed into the picosecond region, and the spin chemistry of such RPs may be exploited for investigating the kinetics of chemical processes on the picosecond time scale.

After the first experimental effects of this kind were discovered[8,9] in the photoinduced electron transfer reaction of $[Ru(bpy)_3]^{2+}$ with methyl viologen (MV^{2+}), our laboratory has systematically explored the effect experimentally[10−13] and theoretically.[14,15] The connection between spin processes and chemical kinetics in the $Ru(bpy)_3^{2+}/MV^{2+}$ system is represented by Scheme 1. The essential point is spin conservation during the chemical reaction steps of forward electron transfer from the photoreactive ^{3}MLCT state of the complex to the electron

* Corresponding author. Fax: ++49 7531 88 3014. E-mail: ulrich.steiner@uni-konstanz.de.

† Part of the special issue "Noboru Mataga Festschrift".

‡ Present Address: European Bioinformatics Institute, Genome Campus, Hinxton, Cambridge CB10 1SD, United Kingdom.

SCHEME 1

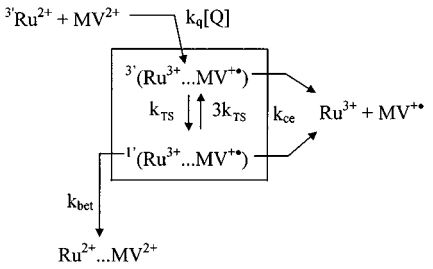

acceptor MV^{2+} and of geminate backward electron transfer from the $MV^{+\bullet}$ radical to the Ru(III) complex in the primary electron transfer product that, as a pair of two $S = 1/2$ systems, essentially represents a radical pair.

The constraint of spin conservation in the second (backward) electron transfer step that regenerates both reactants in their singlet ground states necessitates a multiplicity change of the radical pair because it originates with triplet spin correlation. Thus, a spin process connects the sequence of the two electron transfer reactions. Because the thermodynamic driving force for backward electron transfer is strong, yet not so strong as to put it too far into the Marcus inverted region, the spin-allowed backward electron transfer should be very fast. It is due to the slower spin process that a sizable fraction of the radicals can escape from geminate recombination and be observed as free radicals. Modulating the rate of the spin process by an external magnetic field will affect the efficiency of backward electron transfer *and* of free radical formation. From the MFE on the free radical yield, detailed information about the rate constant of all geminate processes can be deduced. By this method, the absolute determination of very large rate constants is possible even though the radicals are observed on the nanosecond to microsecond time scale. By scavenging the Ru(III) complex with a sacrificial electron donor,[9] it is even possible to conserve the picosecond information encoded in the MFE for many seconds, i.e., as long as the $MV^{+\bullet}$ radicals persist. Aside from homoleptic and heteroleptic complexes of the $[Ru(bpy)_3]^{2+}$ type, the effect has also been investigated with ferrocenes.[16] Our research in this area has benefitted from several collaborations.[15,17−19] Recently it has even been possible to probe in real time the magnetic field induced modulation of an electron transfer process on the time scale of a few picoseconds.[16,20]

To date, few other research groups have independently investigated these extreme spin chemical systems.[21−27] Thus the consequences of the spin chemistry of $Ru(bpy)_3^{2+}$-type complexes have not been fully realized in other areas of chemistry, even though the $Ru(bpy)_3^{2+}/MV^{2+}$ system is "the model system for the photosensitized reduction of water that serves as the prototype against which all others are compared".[28,29] In traditional mechanistic studies of photoinduced electron transfer, the aspect of spin multiplicity in geminate radical pairs is generally neglected and the rate constants of geminate backward electron transfer are evaluated from the efficiency φ_{ce} of free radical formation (cage escape) using the simple relation

$$\varphi_{ce} = \frac{k_{ce}}{k_{ce} + k_{bet}} \qquad (1)$$

By using absolute values of k_{ce} as estimated from diffusion models, absolute values of k_{bet} can be obtained. While this may yield realistic values of k_{bet} for singlet reactions, for triplet reactions these k_{bet} values are at best effective values of backward electron transfer.[19] Questions remain as to what extent they are determined by the rate of spin processes and to what extent by the rate of the backward electron transfer itself.

In 1996, Clark and Hoffman[30] investigated the temperature dependence of φ_{ce} for the $Ru(bpy)_3^{2+}/MV^{2+}$ system and evaluated among other parameters the temperature dependence and activation parameters for k_{bet} in this system. In the present work we report investigations of the temperature and magnetic field dependence of φ_{ce}, as well as of the paramagnetic relaxation time τ_s of the oxidized $[Ru(bpy)_3]^{3+}$ complex in this system. The analysis of these data clearly shows that the temperature dependence of τ_s has a dominant effect on the temperature dependence of φ_{ce} and its magnetic field dependence, and that the rate of backward electron transfer in the geminate RP is essentially determined by the spin process.

2. Material and Methods

2.1. Sample Preparation. $[Ru(bpy)_3](PF_6)_2$ (tris(2,2′-bipyridine)-ruthenium(II)-di(hexafluorophosphate)) was prepared according to a procedure developed at the chemistry department of the University of Fribourg, Switzerland.[31] The laser flash photolysis experiments were carried out in aqueous solutions using deionized water with 2.0×10^{-5} M of the Ru complex and 2.5×10^{-3} M methyl viologen (purum, Fluka). The solutions were adjusted to an ionic strength of 0.1 M by adding sodium chloride (Solvay >98%). All solutions were freed from oxygen by bubbling with nitrogen gas (5.0, Sauerstoffwerk Friedrichshafen).

Solvent viscosities for all temperatures relevant to the MFE measurements were determined using a falling ball viscosimeter (Haake, model C).

$[Ru(bpy)_3]^{3+}$ for the NMR experiments was obtained by in situ oxidation with PbO_2 (Riedel de Haen, 99%). For this purpose, 25−30 mg of $[Ru(bpy)_3](PF_6)_2$ was dissolved in 0.9 mL of CD_3CN (acetonitrile-d_3, Aldrich, 99.6% D) and 0.1 mL D_2SO_4 (98% sulfuric acid-d_2, Aldrich, 99.5% D) and some 50 mg of PbO_2 added. The color of the solution quickly changed from red to green. After 1 h of stirring, excess PbO_2 and precipitated $PbSO_4$ were allowed to settle and 0.5 mL of the supernatant solution was taken up with a syringe and transferred to the NMR tube.

2.2. NMR. ^{1}H NMR measurements were performed in CD_3CN on a JEOL JMN-GX 400 MHz FT spectrometer. The frequency window was set to 50 kHz (125 ppm). Typically 64 scans, each with 16 384 data points, were accumulated at pulse intervals of 1 s. The ppm scales of all spectra were referred to the solvent peak of CD_3CN as 1.93 ppm. Sample concentrations were about 0.05 M. ^{1}H NMR T_1 times were determined by the inversion recovery technique. The time delays Δt between the π and $\pi/2$ pulse were varied between 1 μs and 1 s in intervals of 15 equal steps on a logarithmic time scale. The T_1 times were obtained by fitting the peak values $I(\Delta t)$ to the equation

$$I(\Delta t) = I_0(2f \exp(-\Delta t/T_1) - 1) \qquad (2)$$

where the factor f was introduced to account for the dead time between the $(\pi/2)_x$ pulse and the beginning of the FID signal, due to which the initial signal intensity I_0 does not reach the full negative value of the equilibrium magnetization.

2.3. Nanosecond laser Flash Photolysis. These experiments were carried out using a dye laser (Lambda Physik FL 2000) optically adapted to pumping by the third harmonic (355 nm) of a Nd:YAG laser (Spectra Physics Quanta Ray GCR 150, repetition rate 5 Hz, pulse width ca. 5 ns). Coumarin 47 (Radiant Dyes) in methanol (Merck, p. A.) was used as the laser dye.

The dye laser was tuned to 454 nm. The dye laser beam had a cross section of about 5 mm^2, and the pulse energy was adjusted to 7.7 ± 0.4 mJ. The laser beam and the probe light beam crossed in the probe cell at an angle of about 7°. The detection system comprised a pulsed Xe-lamp (Osram XBO 150) with a home-built power supply, a f/3.4 monochromator (Applied Photophysics), and a Hamamatsu R955 photomultiplier. The signal was recorded with a LeCroy 9354A digital oscilloscope and transferred to a PC equipped with customized software for monitoring and data analysis. A home-built trigger generator was used to control the clock time and the synchronization of all elements active in the measurement. The sample was contained in a cylindrical flow cell of quartz glass with an optical path length of 10 mm and fixed in a temperature-controlled support. The sample solution was delivered in a temperature-controlled flow line, and the temperature of the sample solution was adjusted between 5 and 69 °C. The temperature in the cell was calibrated by a type-K thermocouple. During measurements the flow rate was adjusted such that a full replacement of the cell contents was achieved after three laser shots. The cell was positioned between the pole pieces of an electromagnet (Bruker B−E 15, power supply B-MN C5). The magnetic induction, varied between 0 and 2.9 T, was measured by a Bell Inc. model 615 Gaussmeter with an FTR1−0415 Hall probe. For details of the laser apparatus see ref 32.

Quenching rate constants k_q of the $Ru(bpy)_3^{2+}$ triplet were determined by recording the luminescence decay at 610 nm. Exponential fits of the decay curves yielded the effective decay constants k_{eff} that were analyzed on the basis of the Stern−Volmer relation

$$k_{eff} = k_0 + k_q[MV^{2+}] \tag{3}$$

where k_0 denotes the decay constant in quencher-free solution.

The cage escape yield φ_{ce} of radicals, i.e., the net efficiency of electron transfer, was determined by the saturation method, detecting the $MV^{+\bullet}$ absorption at 395 nm as a function of the laser energy and extrapolating to saturation by the following equation:[33]

$$\Delta A_{395} = \Delta A_{395,sat}(1 - \exp(-bI_L)) \tag{4}$$

where I_L denotes the relative energy of the laser pulse and b is a fit parameter that should be proportional to the extinction coefficient of the irradiated complex at the wavelength of the laser. The value of ΔA_{395} was determined by averaging the signal intensity over a time range where the signal intensity was essentially constant after all ΔA contributions due to the fact that unquenched triplet had decayed. Typical ranges are 1.2−1.7 μs at 5 °C and 0.3−0.5 μs at 69 °C. For varying the laser energy, a series of transmission filters with 70, 50, 35, 25, 18, 10, and 5% transmission were used. Each value of ΔA_{395} was determined as the average of 8−10 individual signals. From $\Delta A_{395,sat}$, the saturation value of the absorbance change at 395 nm, φ_{ce} was obtained by the expression

$$\varphi_{ce} = \Delta A_{395,sat}/\eta_q[Ru(II)]_o\Delta\epsilon_{395} \tag{5}$$

where η_q is the quenching efficiency, given by

$$\eta_q = k_q[Q]/(1/\tau_0 + k_q[Q]) \tag{6}$$

$[Ru(II)]_o$ is the total concentration of ruthenium complex, and $\Delta\epsilon_{395}$ is the change of molar absorbance given by $\epsilon_{MV^{+\bullet}} - \epsilon_{MV^{2+}} + \epsilon_{Ru(III)} - \epsilon_{Ru(II)}$ at 395 nm. The main contribution to $\Delta\epsilon_{395}$ is from the $MV^{+\bullet}$ radical cation that exhibits an absorption maximum at this wavelength with $\epsilon_{395} = 39\,100\ M^{-1}\ cm^{-1}$,[34] whereas for MV^{2+} $\epsilon = 0$. The ϵ value of $[Ru(bpy)_3]^{3+}$ was measured after in situ oxidation of $[Ru(bpy)_3]^{2+}$ in acidified solutions ($[H_2SO_4] = 0.5$ M) by PbO_2. The following values were obtained: $\epsilon_{Ru(III)} = 1800\ M^{-1}\ cm^{-1}$ and $\epsilon_{Ru(II)} = 5700\ M^{-1}\ cm^{-1}$.

The relative MFE on φ_{ce} was measured by comparing ΔA_{395} for experiments with and without a magnetic field averaging 20−30 signals in each case. The field effect $R_{\varphi ce}(B_0)$ is defined as

$$R_{\varphi_{ce}}(B_0) \equiv \frac{\Delta A_{395}(B_0) - \Delta A_{395}(B_0 = 0)}{\Delta A_{395}(B_0 = 0)} \tag{7}$$

2.4. Computer Simulations. For numerical simulations of the spin-dependent reaction dynamics outlined in Scheme 1, a program package QYIELD written in C++ code was developed.[35] It is based on theoretical work published in refs 10, 14, 15, 36, 37 and solves the stochastic Liouville equation (SLE) of the spin density matrix of the RP. For describing the spin dynamics, the g-tensor values $g_{||}$ and $g_\perp$ of the Ru(III) moiety and its spin relaxation time τ_S (where $\tau_S = T_1 = T_2$ is assumed) are required as input parameters. For dealing with the diffusional dynamics of the RP, two options are provided: (i) description in terms of a radially symmetric continuous diffusion/reaction equation where the rate constant of backward electron transfer is explicitly treated as a distance dependent, exponentially decaying function; (ii) description in terms of the so-called exponential model,[38] where the transition between RP in contact and free radicals is described by a first-order rate constant k_{ce} and the spin-allowed recombination by a rate constant k_{bet}. The analysis of the MFEs in this paper were mainly based on the exponential model.

The program provides a fitting routine for the three kinetic parameters k_{ce}, k_{bet}, and τ_S. It minimizes the mean square deviation between experimental and theoretical function $\varphi_{ce}(B_0)$ by using a standard Newtonian minimization with global search strategy.[39] Furthermore, it provides an option to calculate the isolines of the root-mean-square (rms) deviation in a 2-D field of any two of the three parameters k_{ce}, k_{bet}, and τ_S, with one of them kept fixed. Such diagrams provide instructive visualizations of the extent of variability that the fitting procedure allows for the values of the fit parameters.

3. Results

3.1. Paramagnetic NMR. The complete assignment of the paramagnetic ^1H NMR spectra of the trisbipyridine and the trisphenanthroline complexes of the trivalent metals of the iron group have been given by De Simone and Drago.[40] These authors were mainly interested in the evaluation of isotropic hyperfine coupling constants of these compounds and did not measure the T_1 times of the protons, although they noted a qualitative (negative) correlation of the NMR line widths with the distance of the protons from the paramagnetic center. The temperature-dependent values of chemical shifts and T_1 times of the equivalent pairs of protons are given in Table 1 (for the numbering of the protons, see Figure 1).

The Curie plots for the δ-values yield excellent straight lines. In principle, the intercepts should represent the values of the diamagnetic reference compounds and might be used to support the assignments of the proton. However, the accuracy of this extrapolation is not sufficient for a safe assignment on this basis. The T_1 values allow a much more reliable assignment. It is in full accord with that of DeSimone and Drago.[40]

TABLE 1: Temperature Dependent ^{1}H NMR Chemical Shift (in ppm), T_1 data (in ms), and τ_c (in ps) of $[Ru(bpy)_3]^{3+}$

	H (3,3')		H (4,4′)		H (5,5′)		H (6,6′)		
T, K	δ	T_1	δ	T_1	δ	T_1	δ	T_1	τ_c
314.9	15.45	10.36	−0.30	18.27	8.30	10.48	−28.60	0.95	16.3
304.9	15.80	9.28	−0.50	16.68	8.20	9.51	−30.20	0.89	17.9
294.3	16.00	8.42	−0.75	15.32	8.20	8.64	−31.80	0.78	19.8
284.5	16.30	7.41	−1.00	13.48	8.20	7.67	−33.50	0.71	22.4
274.5	16.65	6.80	−1.20	12.11	8.10	6.96	−35.50	0.63	24.7
264.5	16.90	5.76	−1.40	10.64	8.10	6.01	−37.00	0.55	28.6
254.5	17.20	5.21	−1.55	9.44	8.20	5.29	−38.00	0.49	32.3
244.5	17.70	4.51	−1.90	8.22	8.10	4.64	−41.00	0.42	37.1
234.3	18.05	3.88	−2.15	7.11	7.90	4.03	−43.00	0.37	43.0

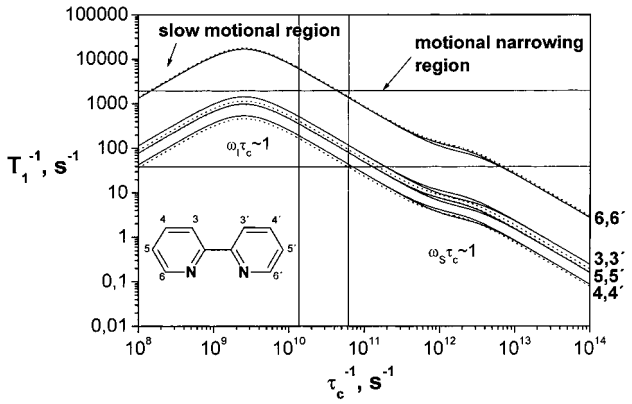

Figure 1. Curves representing the theoretical relation between ^{1}H T_1 times for specified ligand protons and electronic correlation time τ_c according to the Solomon eq 6 (dotted lines) and the relations due to Bertini et al.[44] and Vasavada and Rao[45] (solid lines). The latter curves differ only in the region $\omega_S\tau_S \approx 1$, where T^{-1} according to Vasavada and Rao is somewhat higher. The Solomon curves for protons 5,5′ and 6,6′ are practically identical with the solid lines calculated after Bertini et al., while they are somewhat below the more refined results for the 3,3′ and 4,4′ protons.

In paramagnetic compounds, not only the chemical shifts but also the nuclear relaxation times are dominated by the dipolar interaction between electronic and nuclear spins.[41] The basic relation has been derived by Solomon.[42] For $S = 1/2$, it reads

$$T_1^{-1} = \frac{1}{10}\left(\frac{\mu_0}{4\pi}\right)^2 \frac{\hbar^2\gamma_I^2\gamma_S^2}{r^6}\left[\frac{7\tau_c}{1+\omega_S^2\tau_c^2} + \frac{3\tau_c}{1+\omega_I^2\tau_c^2}\right] \quad (8)$$

Here μ_0 is the magnetic permeability constant of the vacuum, γ_I and γ_S are the magnetogyric ratios of proton and electron, respectively, r is the electron−proton distance, τ_c is the correlation time of the electron−nuclear dipolar magnetic interaction, and ω_S and ω_I are the Larmor frequencies of electron and proton, respectively. For paramagnetic complexes in dilute solutions, the correlation time τ_c is, in general, composed of two contributions:

$$\tau_c^{-1} = \tau_R^{-1} + \tau_S^{-1} \quad (9)$$

where τ_R is the rotational correlation time and τ_S the correlation time of the electron spin. Equation 8 is strictly applicable only for systems with an isotropic g-factor. For $[Ru(bpy)_3]^{3+}$, the g-tensor is axially symmetric. Measurements in our laboratory yielded $g_\parallel = 1.18$ and $g_\perp = 2.60$.[43] These values are in good agreement with those given by DeSimone and Drago ($g_\parallel = 1.14$ and $g_\perp = 2.64$).[40]

For systems with an anisotropic g-tensor, generalizations of eq 8 have been derived by Bertini et al.[44] and by Vasadava and Rao.[45] While the result of the former is applicable to systems with axial g-tensor and having $\tau_R \gg \tau_S$, the result of the latter applies to systems with rhombic g-tensor and $\tau_R^{-1} \gg \tau_S^{-1}$. Furthermore, it takes isotropic hyperfine coupling into account. For anisotropic g-tensor, the nuclear relaxation times depend not only on the electron−nuclear distance but also on the angular position of the nuclear spin in the molecular frame. The coordinates of the protons in $[Ru(bpy)_3]^{3+}$ from X-ray crystallographic data[46] are given in Table 2.

TABLE 2: Geometric Coordinates of the Protons in the Molecular Axis System of $[Ru(bpy)_3]^{3+}$

proton	θ, deg[46]	r, Å[46]	r_{eff}, Å[a]	Δr, Å[b]
3,3′	77.74	4.942	5.100	+0.16
4,4′	57.26	5.748	5.560	−0.19
5,5′	42.26	5.078	4.938	−0.14
6,6′	37.36	3.132	3.275	+0.14

[a] Distance from the center that should be chosen in order that the τ_S values for all protons coincide with the average τ_S value. [b] $\Delta r = r_{eff} - r$.

By using the g-tensor and the geometric data, the dependences of the T_1 times of the various protons as a function of the correlation time τ_c can be predicted. In Figure 1 the curves calculated with the relations of Bertini et al.[44] and Vasavada and Rao[45] are shown together with the curves corresponding to the simple Solomon eq 8.

The two terms in the Solomon eq 8 are contributed from spin transitions where only nuclear spins are changed (ω_I term) or when both electronic and nuclear spins are changed (ω_S term). Each of these terms yields a curve with an increasing branch ($\omega\tau_c > 1$, "slow motional" region) and a decreasing branch ($\omega\tau_c < 1$, "motional narrowing" region) with a maximum at $\omega\tau_c = 1$. Since the maximum value of T_1^{-1} is proportional to $\tau_c = 1/\omega$, the higher contribution is found for $\tau_c = 1/\omega_I$. As the $T_1^{-1}(\tau_c^{-1})$ curves are non-monotonic, measuring T_1 does not lead to a unique assignment of τ_c. However, because it can be reasonably expected that τ_c^{-1} increases with temperature, we can judge from the negative temperature dependence of T_1^{-1} that our system is in the motional narrowing region, and to any T_1 observed, a unique τ_c value can be assigned (see Figure 1).

The differences between the curves from the simple Solomon equation and the more refined treatments are subtle (Figure 1). For protons 5,5′ and 6,6′, the angular position is such that they feel to a very good approximation the average g-factor used in the Solomon equation. For the other protons that are closer to the main axis of the complex, the effective g-factor is smaller (closer to the axial value) than the isotropic average value and the $T_1^{-1}(\tau_c^{-1})$ curves are shifted somewhat downward, especially for protons 3, 3′. For the $[Ru(bpy)_3]^{3+}$ complex, the curves according to Bertini et al.[44] and to Vasavada and Rao[45] differ only in the region where $\omega_S\tau_c \sim 1$, i.e., where combined nuclear and electronic spin transitions have their maximum contribution to spin relaxation. However, since isotropic hyperfine coupling constants are less than 0.2 G for all the protons in the complex, this small difference is not relevant in the range of T_1^{-1} values measured for our system.

Strictly speaking, each proton should probe the same value of τ_c. From Figure 2, for the given geometry, the τ_c values of the different protons show some distribution within ±25% of their average. However, these deviations are systematic and do not depend on the temperature. The assignment of the chemical shift values of the protons as given in Table 1 (and in agreement with DeSimone and Drago[46]) corresponds to the case where the deviation of the individual τ_c values is smallest.

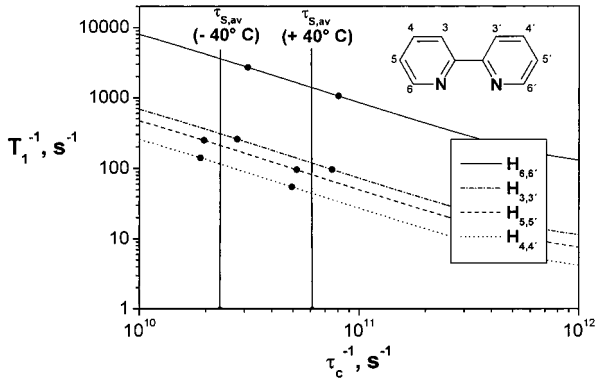

Figure 2. Illustration of τ_c evaluation from the experimental T^{-1} values for the four sets of protons at the extremes of the temperature range investigated.

To seek a better understanding of the uncertainty of τ_c, we investigated the error propagation in the determination of τ_c from T_1 on small variations of the magnetic and geometric parameters, viz. of $\Delta g \equiv (g_\perp - g_\parallel)$, of r_i, and of θ_i. The results depend on the position of the particular proton:

$$\left(\frac{\partial \ln \tau_c}{\partial \Delta g}\right)_{T_1} = 0.21...0.34$$

$$\left(\frac{\partial \ln \tau_c}{\partial r_i}\right)_{T_1} = 1.04...2.07\ \text{Å}^{-1}$$

$$\left(\frac{\partial \ln \tau_c}{\partial \theta_i}\right)_{T_1} = -0.002...-0.012\ \text{deg}^{-1}$$

From these values it is clear that the evaluation is most sensitive to the radial distance of the proton from the center. In Table 2 we present effective values of r_i that would be required for all τ_c values to coincide with the average value of all protons at each temperature. The deviations from the actual crystallographic values are less than 0.2 Å in each case. The observed deviations may be due to the shortcoming of the point dipole approximation that lies at the basis of the r^{-6} dependence of T_1^{-1}.

The temperature variation of τ_c ranges from 43 ps at 233 K to 16 ps at 315 K. It is by 1 order of magnitude smaller than τ_R (see ref 47). From this we conclude that the correlation time τ_c of the electron−nuclear interaction is almost exclusively due to the electron spin correlation time τ_S. Hence the electron spin relaxation must be caused by a mechanism that is independent of molecular rotation. In the following it will be assumed that $\tau_c = \tau_S$ and that $\tau_S = T_{1,s} = T_{2,s}$ (see Discussion).

3.2. Magnetic Field Effects. Typical transient absorption signals recorded for the quenching of $*[Ru(bpy)_3]^{2+}$ by MV^{2+} at different temperatures are shown in Figure 3. The fast signal rise during the laser pulse is due to the excited-state absorption of $*[Ru(bpy)_3]^{2+}$, the slower one, on the time scale of several 100 ns, is due to the creation of $MV^{+\bullet}$ radicals in the quenching process. The time constant of this process is the same as that for the luminescence decay of $*[Ru(bpy)_3]^{2+}$. The increase of the quenching rate constant with increasing temperature is clearly apparent from the rise times of the signals shown in Figure 3 (note the different time scales in the two panels of the figure).

The plateau of ΔA reached after the quenching is completed marks the yield of free radical formation in the quenching process. Since the concentrations and the laser energy were kept

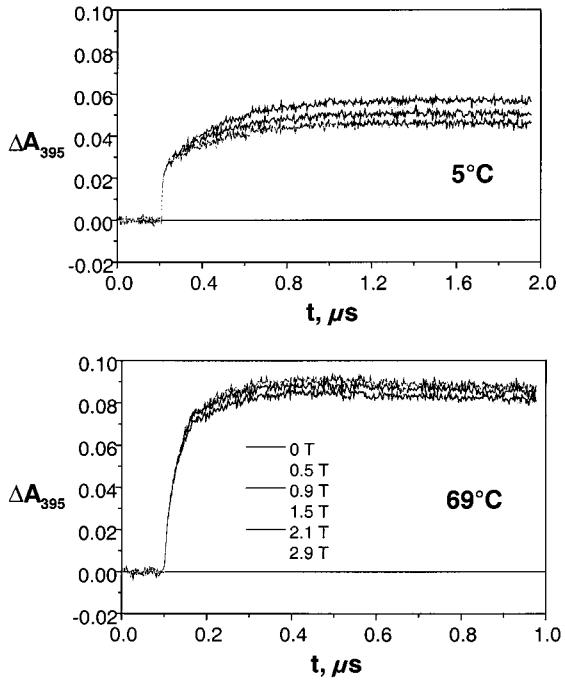

Figure 3. Transient absorption signals detected at 395 nm (maximum of the $MV^{+\bullet}$ radical absorption) for 5 °C and 69 °C in different magnetic fields. The indicated set of magnetic fields applies to both temperatures. The signal amplitudes decrease monotonically with the field. Each signal represents an average over 30 laser shots. $[MV^{2+}] = 2.5$ mM, $[Ru(bpy)_3]^{2+} = 2.0 \times 10^{-5}$ M.

TABLE 3: Temperature Dependence of Observed Quantities and Evaluated Kinetic Parameters for the Quenching of $*[Ru(bpy)_3]^{2+}$ by Methyl Viologen[a]

T °C	$1/\eta$ cP^{-1} [b]	k_q ns^{-1} M^{-1}	φ_{ce}	k_c ns^{-1}	k_{bet} ns^{-1}	τ_S ps	$k_{TS} = (4\tau_S)^{-1}$ ns^{-1}	$k_{bet,eff}$ ns^{-1}
5	0.65	0.8	0.16	1.3	55	31	8	7
15	0.87	1.0	0.17	1.7	69	26	10	9
20	0.98	1.1	0.18	2.0	73	24	11	9
25	1.11	1.2	0.18	2.2	79	21	12	10
33	1.32	1.5	0.19	2.6	86	18	14	11
42	1.57	1.8	0.20	3.1	97	15	16	13
52	1.87	2.1	0.21	3.7	107	14	18	14
61	2.14	2.4	0.22	4.3	114	12	21	16
69	2.39	2.7	0.23	4.8	116	12	22	16

[a] The fit values of k_{bet} and τ_S were determined by using the refined values of k_{ce} employing the assumption $k_{ce} \propto 1/\eta$ (see text). For standard errors see Figures 4 and 6 and the comment in ref 50. [b] Viscosity of water with an ionic strength of 0.1 M (NaCl).

constant, it is evident from Figure 3 that the yield of free radicals increases with temperature. The efficiency φ_{ce} of cage escape has been determined by measuring the laser-intensity dependence of ΔA and the quenching constant k_q (see Experimental Section). The φ_{ce} values at different temperatures are given in Table 3.

There is good general agreement between the previously published values by Clark and Hoffman[30] and our results (see Figure 4). Our data cover a somewhat wider interval of temperatures and show a smoother variation. As can be seen in Figure 3, the signal amplitude is magnetic field dependent. It has been demonstrated in detail in ref 9 that this effect is due exclusively to the magnetic field dependence of φ_{ce}, which decreases as the magnetic field is increased. To our knowledge, the temperature dependence of magnetic field effects with unlinked radical pairs has not been investigated to date. As shown in Figure 5, the relative magnetic field effect on φ_{ce}, defined as

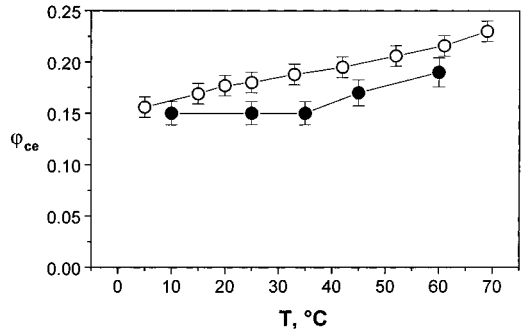

Figure 4. Cage escape efficiency φ_{ce} as a function of temperature. Open circles: this work; closed circles: data from Clark and Hoffman.[30]

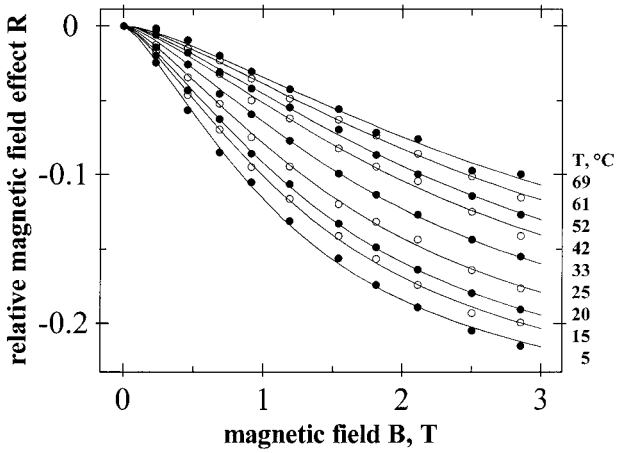

Figure 5. Relative magnetic field effect R of cage escape efficiency as a function of magnetic field. The data points represent average values from five to eight experiments, each of them averaging the signals of 30 laser shots. The lines represent the best fits obtained by a three-parameter optimiziation (for details see text).

$$R_{\varphi_{ce}}(B_0) = \frac{\varphi_{ce}(B_0) - \varphi_{ce}(0)}{\varphi_{ce}(0)} \tag{10}$$

exhibits a marked temperature dependence. The field effect decreases as the temperature increases. It should be clear that, compared to the situation where only the value of φ_{ce} at zero field is available for each temperature, the accessibility of the magnetic field dependence of φ_{ce} at each temperature represents a significant increase of information on the kinetics of the system. Actually, with the magnetic field dependence a full further dimension becomes available. It is equivalent to observing the radical pair with a time resolution of some picoseconds (see Discussion).

The analysis of the MFE was carried out on the basis of the reaction mechanism represented in Scheme 1. Here the rate constants of k_{ce}, k_{bet}, τ_s are defined. They characterize the kinetics of radical pair dissociation (cage escape), spin-allowed backward electron transfer, and spin conversion, respectively. For spin-statistical reasons the rate constant of singlet-to-triplet conversions must correspond to three times the rate constant of triplet-to-singlet conversion. The NMR results demonstrated that spin relaxation at the Ru(III) center is a very fast process. Actually, it is this process that determines the S/T or T/S conversion of the geminate redox pair $[Ru(bpy)_3]^{3+}/MV^{+\bullet}$. It can be shown that k_{TS} is related to τ_s by[14,49]

$$k_{TS} = (4\tau_S)^{-1} \tag{11}$$

The theoretical treatment of the reaction kinetics employed here corresponds to a standard first-order reaction kinetic treatment of Scheme 1. It includes, however, the additional feature of the coherent magneticfield induced T/S and S/T transitions that are caused by the different Larmor precession frequencies of the spins at the Ru(III) center and at the $MV^{+\bullet}$ radical. The characteristic quantities to be used here are the g-tensor components of the $[Ru(bpy)_3]^{3+}$ complex ($g_{\|} = 1.18$and $g_{\perp} = 2.60$)[43] and of the $MV^{+\bullet}$ radical ($g = 2.00$). The strongly anisotropic g-tensor of $[Ru(bpy)_3]^{3+}$ indicates efficient mixing of different spin−orbit states. The spin is therefore not a good quantum number for this species and has to be replaced in the spin Hamiltonian by the effective spin. As a consequence, the formal substates of the electronic ground multiplet of the radical pair cannot be assigned sharp spin values either. As has been shown,[14] the formal spin substates S′, $T_{\pm}$′, T_0′ (where the prime denotes that they are composed of effective $S = 1/2$ components) of the RP can be assigned singlet characters p_i′ that are related to the g-tensor components of the Ru(III) moiety. For $[Ru(bpy)_3]^{3+}$, the assignments are $p_{S'} = 0.858$, $p_{T_{\pm}'} = 0.071$, and $p_{T_0'} = 0.0$. We use these to differentiate the backward electron transfer rate constants of these substates as

$$k_{bet,i'} = p_{i'} k_{bet} \tag{12}$$

All the specifications just described enter the various terms of the stochastic Liouville equation (SLE) for the spin density matrix ρ of the radical pair:

$$\dot{\rho}(t) = -\frac{i}{\hbar}[H,\rho]_- + \mathscr{R}\rho - \frac{1}{2}[K,\rho]_+ \tag{13}$$

where $[\ ]_-$ and $[\ ]_+$ denote the commutator and anti-commutator, respectively, H is the Zeeman spin Hamiltonian (characterized by the g-values), $\mathscr{R}$ is the relaxation super operator (characterized by the spin correlation time τ_S and assuming $\tau_S = T_1 = T_2$ for the effective spin of the Ru(III) center), and K the reaction operator (characterized by k_{ce}, k_{bet}, and the $p_{i'}$). From the time-integrated solution $\int_0^\infty \rho(t)\, dt$ calculated for a random orientational distribution of the Ru(III) complexes and isotropically averaged, we obtain the efficiency of cage escape $\varphi_{ce}(B_0)$ as a function of the magnetic field.[14,49]

For each temperature represented in Figure 5, the parameter set k_{ce}, k_{bet}, τ_S was determined by fitting the theoretical dependence of $\varphi_{ce,calc}(B_0)$ to the observed data. A general fitting routine minimizing the rms deviation between experimental and theoretical data was implemented in the computer program. It must be emphasized that no preinformation or physical restraint for these parameters enters the fitting procedure at this stage. The resulting best fit curves yield an excellent representation of the experimental $\varphi_{ce}(B_0)$ data (see Figure 5). The temperature dependence of the parameters together with their standard errors[50] are represented in Figure 6.

To obtain a quantitative representation of the degree of ambiguity inherent in the determination of the kinetic parameters from the fitting of the MFE curves, we plotted the lines of constant rms deviation of the fits for each pair of the three parameters with the third parameter kept fixed. For $T = 5$ °C these iso-rms line maps are shown in Figure 7a−c. What is apparent from them is the elongated elliptic shape of the isolines that is rather extreme in the case of the k_{bet}/k_{ce} plane. It means that along the long axes of these ellipses the effects of the two parameters on the $\varphi_{ce}(B_0)$ curve largely compensate each other. If one takes this property into account, the ambiguity of the fits is wider than estimated with the propagation scheme of independent errors (see ref 50). If we set a relative rms value

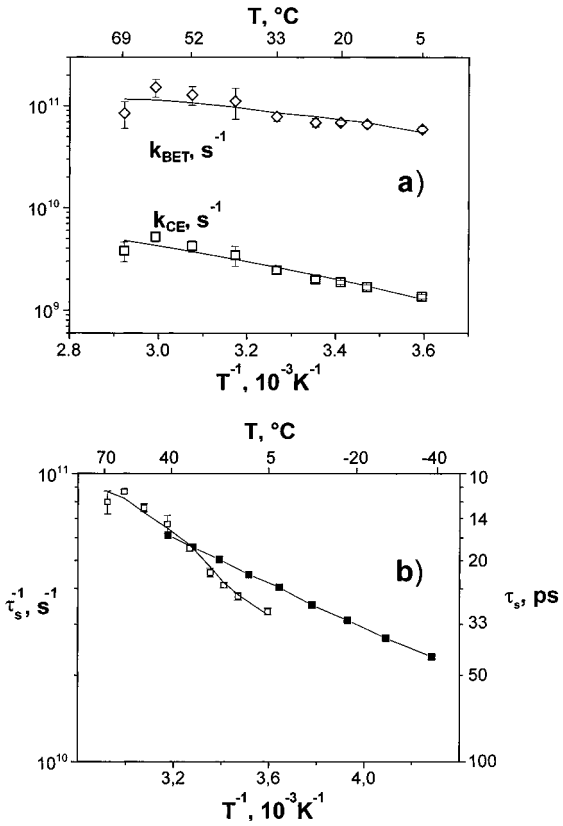

Figure 6. Rate constants k_{ce}, k_{bet} (a), and τ_S (b) as a function of temperature: open symbols with error bars. The solid line for k_{ce} represents the best fit of the function $k_{ce} = A/\eta$ to the k_{ce} data points. Here A is a fit parameter and η the solvent viscosity. The solid lines for k_{bet} and τ_S result from a two-parameter fit of the MFE curves with k_{ce} fixed to the viscosity-adapted value. The solid symbols in panel (b) represent the τ_c values determined by the NMR experiments.

of about 1% as the limit of a significant deviation between experimental and calculated $\varphi_{ce}(B_0)$ data, we obtain the limits of acceptable parameter values given in Table 4 for 5 °C (see Figure 7a−c).

For each of the parameters the admissible variation covers a factor of ∼1.5. In the case of the k_{bet}/k_{ce} compensation the parameter variation is a factor of ∼3.5. This may seem quite large. However, when taking into account that no preinformation on any of the parameters was used, it is still a fairly good kinetic assessment of the system in absolute terms. Furthermore, the parameter values cannot be selected in an uncorrelated way out of the given ranges but are strongly correlated. To narrow the admissible ranges of the parameter values we introduce a plausible physical constraint. In their spin-free analysis of φ_{ce}, Clark and Hoffman[30,51] assessed the value of k_{ce} by employing the absolute value predicted by the Eigen−Debye equation.[52] We will assume only the proportionality of k_{ce} to the relative diffusion coefficients of the two radical moieties, i.e., within the Stokes−Einstein approximation, to the inverse of solvent viscosity η that has been measured for all temperatures (see Table 3). In fact, the temperature dependence of $1/\eta$ correlates well with that of the k_{ce}values obtained from the global rms deviation minima. Using the relation

$$k_{ce} = \frac{A}{\eta} \tag{14}$$

with a value of $A = 2.0$ ns^{-1}cP we obtain the curve shown in Figure 6a. This curve is used to assign $k_{ce}(T)$ and, by virtue of the correlations established in the diagrams with the isolines of

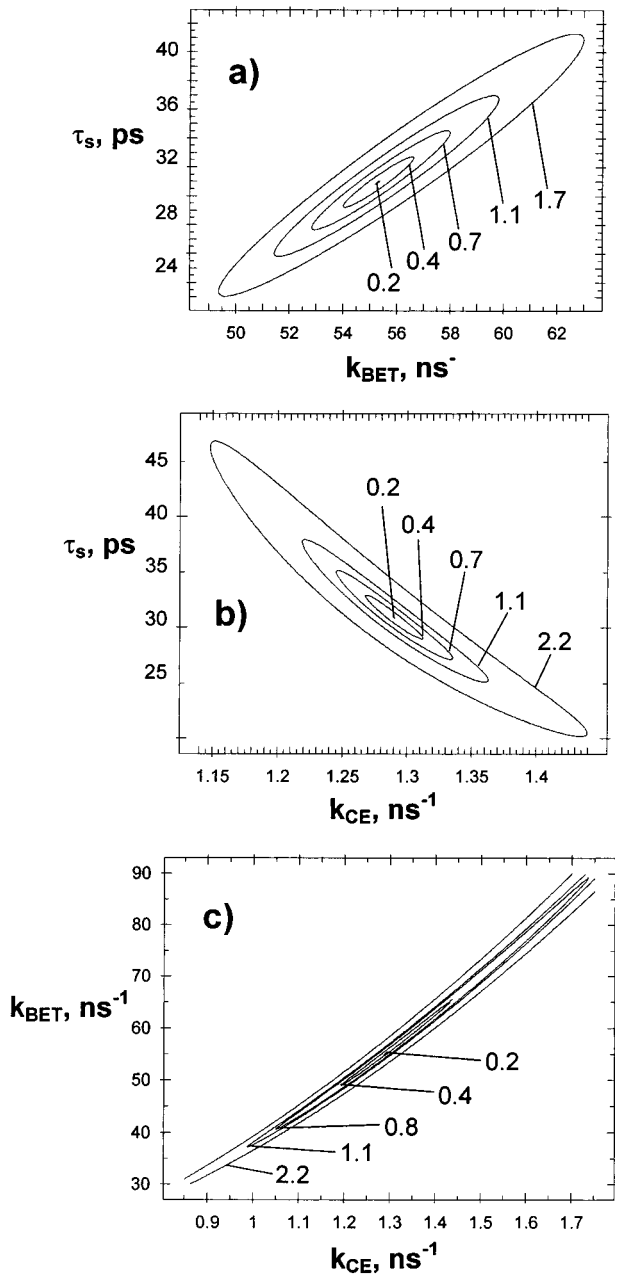

Figure 7. Plots representing lines of constant rms deviation between theoretical and experimental $\varphi_{ce}(B_0)$ values. The numbers given indicate the rms value in percent.

TABLE 4: Ranges of Fit Parameters Yielding Relative rms Values of Less than 1.1% for the Simulated MFE Curves

fixed value	ranges of fit parameters	
$k_{ce} = 1.29$ ns^{-1}	26 ps ≤ τ_s ≤ 36 ps	51 ns^{-1} ≤ k_{bet} ≤ 60 ns^{-1}
$k_{bet} = 55.2$ ns^{-1}	1.22 ns^{-1} ≤ k_{ce} ≤ 1.36 ns^{-1}	25 ps ≤ τ_s ≤ 38 ps
$\tau_s = 30.9$ ps	37 ns^{-1} ≤ k_{bet} ≤ 128 ns^{-1}	0.99 ns^{-1} ≤ k_{ce} ≤ 2.15 ns^{-1}

rms deviations, fixes the values of $k_{bet}(T)$ and $\tau_S(T)$. The resultant temperature-dependent values for all three kinetic parameters are provided in Table 3 and are represented by solid lines in Figure 6. As can be seen here, the "viscosity-adapted" values for the temperature dependence of the parameter values yield rather smooth lines through the data points determined by the three-parameter fitting routine. The slopes of these lines yield the following values for the Arrhenius activation energies: 16 kJ mol^{-1} ≙ 1340 cm^{-1} (k_{ce}, $1/\eta$), 9.1 kJ mol^{-1} ≙ 760 cm^{-1} (k_{bet}), 12.8 kJ mol^{-1} ≙ 1070 cm^{-1} (k_{TS}, $1/\tau_S$). The τ_S^{-1} data

from the NMR experiments (see Table 1) are also plotted in Figure 6b. In this case the slope corresponds to an activation energy of 7.5 kJ mol^{-1}(620 cm^{-1}).

4. Discussion

If the coherent spin motion induced by an external magnetic field is to be fully taken into account, an adequate kinetic treatment of the reaction mechanism represented in Scheme 1 is only possible with the SLE formalism. However, in zero field or for a qualitative account of the MFE, a conventional kinetic treatment in terms of first-order rate processes is appropriate. As has already been explained, singlet character is not restricted to a single substate of the radical pair but is distributed over three of them (S′, T_+′, T_-′) so that each of them has a finite rate constant $p_{i'}\,k_{bet}$ for reacting back to the singlet ground state. Including this general reactivity of the substates, the cage escape efficiency in zero field can be expressed as

$$\varphi_{ce} = \frac{2}{3}k_{ce}\frac{12d^2 + (2a + 4b + 6c)d + ac + 2bc}{(4a + 2b + 2c)d^2 + (3ab + 3ac + 2bc)d + 2abc} \tag{15}$$

with

$$a = p_{T_{\pm}'}k_{bet} + k_{ce}$$

$$b = k_{ce}$$

$$c = p_{S'}k_{bet} + k_{ce}$$

$$d = 2k_{TS}$$

For zero field, eq 15 represents an exact solution. Its results exactly match the numerical solution of eq 13 for zero field. We may proceed to a more transparent analytical expression that allows the qualitative rationalization of various aspects of the MFE, if we consider the limit of $k_{ce} \ll k_{TS}$, k_{bet} and set $p_{S'} = 1$, and $p_{T\pm}{}' = 0$. With these assumptions and using the identity $k_{TS} = (4\tau_S)^{-1}$, eq 15 simplifies to

$$\varphi_{ce} = k_{ce}\frac{1 + \tau_S k_{bet}}{k_{ce}(1 + \tau_S k_{bet}) + \frac{1}{4}k_{bet}} \tag{16}$$

With this result it can be easily shown what a spin-free interpretation of φ_{ce} means, i.e., analyzing it in terms of eq 1. Let us define an effective rate constant $k_{bet,eff}$ as

$$k_{bet.eff} \equiv k_{ce}\frac{1 - \varphi_{ce}}{\varphi_{ce}} \tag{17}$$

Then we obtain from eq 16

$$k_{bet.eff} = \frac{1}{4}\frac{k_{bet}}{1 + \tau_S k_{bet}} \tag{18}$$

It is easy to see that, depending on the value of $\tau_S k_{bet}$, the value of $k_{bet,eff}$ will range between $(1/4)k_{bet}$ and k_{TS}. The latter limit corresponds to the case when the spin conversion process is rate limiting for the backward electron transfer. According to Table 3, the product $\tau_S k_{bet}$ ranges around 1.5. For this value eq 18 predicts $k_{bet,eff}$ to be only about 1/10 of k_{bet}. The values obtained for $k_{bet,eff}$ by inserting the experimental values of φ_{ce} into eq 17 are listed in Table 3. They are about 30% larger than obtained from approximation (eq 18) but they show exactly the same trend. When comparing the values of $k_{bet,eff}$ with those of k_{TS} for the system under investigation, the values of $k_{bet,eff}$ are close to spin-controlled, i.e., what was taken to correspond to the rate constant of backward electron transfer in refs 30 and 54 is actually closer to the rate constant of the spin conversion process than to that of the electron transfer step proper.[53]

To understand the MFE qualitatively, it is sufficient to know that the substates of the RP are coherently interconverted among each other by virtue of the different Larmor frequencies of the two unpaired spins. The rate of substate interconversion is proportional to the magnetic field. Although this is a coherent process, i.e., it leads to a periodic motion through the spin substates, one can qualitatively describe its effect by interpreting it as an effective increase of k_{TS} (although it should be clear that in the rigorous treatment this quantity is assumed to be field independent, see below). Thus, the magnetic field accelerates the triplet−singlet spin conversion and thereby enhances the backward electron transfer. Consequently, the free radical yield decreases in a magnetic field. To see how the various kinetic parameters affect the magnetic field sensitivity of φ_{ce} we consider the expression

$$R' \equiv \frac{1}{\varphi_{ce}}\left(\frac{\partial\varphi_{ce}}{\partial k_{TS}}\right)_{k_{ce},k_{bet}} \tag{19}$$

For the purpose of a qualitative interpretation, R' should be a good indicator of the sign and size of the MFE R. By using the simplified expression (eq 14) for φ_{ce}, we obtain in the limit of small k_{ce}:

$$R' = -4\tau_S\frac{\tau_S k_{bet}}{1 + \tau_S k_{bet}} \tag{20}$$

This shows that the MFE is negative and does not depend on k_{ce} (to first order). It is only sensitive to τ_S and k_{bet}. Increasing k_{bet} affects R' only for values of this parameter that are not too large. If $\tau_S k_{bet} \gg 1$, the sensitivity of R' to k_{bet} becomes saturated. The same does not hold for τ_S. While a quadratic dependence of R' on τ_S prevails for $\tau_S k_{bet} \lesssim 1$, a linear dependence of R' on τ_S remains in the limit $\tau_S k_{bet} \gg 1$. The experimentally observed decrease of the MFE with increasing temperature (see Figure 5) is caused by the temperature dependence of τ_S. The weak increase of k_{bet} with increasing temperature (see Table 3) that should tend to increase the MFE cannot counterbalance the stronger effect due to the decrease of τ_S.

We have emphasized that the present method of exploiting the magnetic field dependence of φ_{ce} is superior to the evaluation of φ_{ce} only at zero field. From the magnetic field dependence the absolute values of the rate constants k_{ce}, k_{bet}, and k_{TS} can be assessed. Although our present measurements did not employ a time resolution matching the rate constants in real time,[55] the physical dimension of the magnetic field strength provides an internal "Larmor clock" through the relation

$$\Delta\omega_L = \frac{\Delta g\mu_B}{\hbar}B_0 \tag{21}$$

where $\Delta\omega_L$ is the difference of the Larmor frequencies of the two spins caused by the difference Δg of their g-factors.[56] With Δg of the order of unity, a magnetic field of 1 T corresponds to a $\Delta\omega_L$ of about 10^{11} rad s^{-1}. Due to the kinetic coupling of spin processes and chemical processes it is possible to "read" the Larmor clock from the MFE on the cage escape efficiency $\varphi_{ce}(B_0)$. In practice, this reading of the Larmor clock amounts to performing a three-parameter fit of the observed $\varphi_{ce}(B_0)$ data.

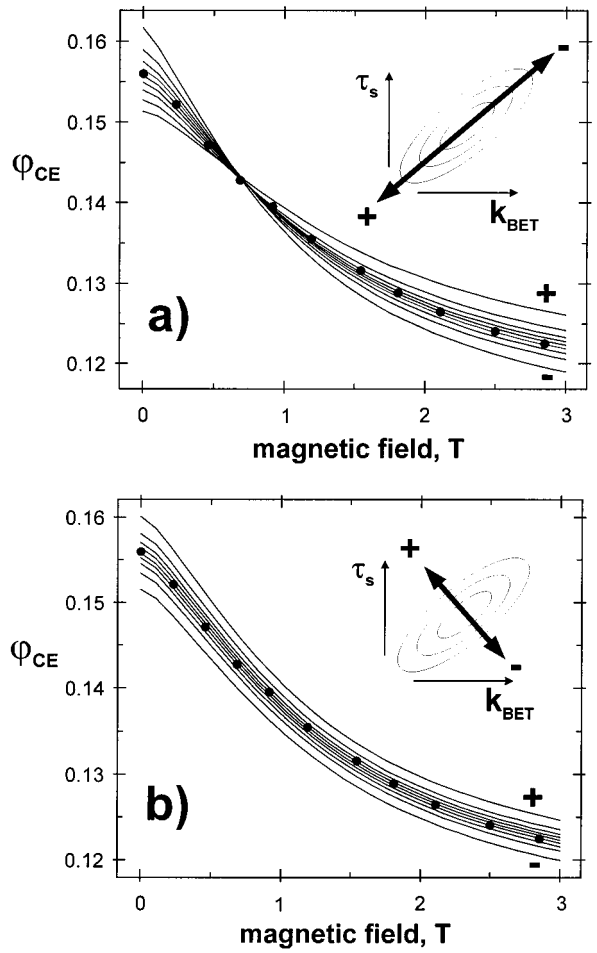

Figure 8. Representation of fit quality for parameter values varied along the long and short axes, respectively, of the iso-rms line ellipses of Figure 7a. While the best fit corresponds to an rms deviation of 0.2%, the set of curves shown in each panel comprises values of 0.33%, 0.6%, 1.1%, and 1.9% for parameter variation in both directions from the best fit. The fit curves with an rms deviation of 1.9% are clearly outside the tolerable range.

The narrowness of the ranges within which the kinetic parameters can be fixed by such a procedure alone, has been illustrated with the rms isoline diagrams in Figure 7. Here the more or less compressed shape of the elliptical contour lines indicates that changes in the kinetic parameters can compensate each other to some extent in their effect on φ_{ce}. If we denote the kinetic parameters k_{ce}, k_{bet}, and k_{TS} by the general symbol k_i, the condition for compensation of two parameters k_i, k_j, i.e., the direction $m_{i,j}$ of the long axis of the corresponding rms isoline ellipse, can be stated as

$$m_{i,j} = \left(\frac{\partial k_i}{\partial k_j}\right)_{k_l,\varphi_{ce},B_0} \tag{22}$$

with all cyclic permutations of the indices i, k, l (i.e., i = ce, k = bet, l = TS). Moving along such a direction will leave φ_{ce} invariant for a certain value of B_0, but not for $\varphi_{ce}(B_0)$ in general. The effect of a parameter variation along the main axis of an rms isoline ellipse is shown in Figure 8a. We note that the predicted φ_{ce} for some central field value remains invariant, but the various $\varphi_{ce}(B_0)$ curves deviate from the correct one in different directions before and after the invariant point. If the two parameters are chosen to vary along the direction of the short axis of the rms isoline ellipse, the effects of the changes of the two parameters enhance each other. The resultant curves exhibit parallel shifts relative to the correct reference curve calculated with the parameter sets corresponding to the centers of the rms isoline ellipses (see Figure 8b).

In general, the uniqueness of the three-parameter fit, i.e., the absence of significant compensation for φ_{ce} as a function of the magnetic field, depends on the experimentally resolved features of the magnetic field dependence, in particular on its initial slope and its curvature. In that respect it would be desirable to scan a field range as wide as possible.[57] The range up to 3 T turns out to give sufficient information for most of the temperatures of the present investigation, although for the highest temperatures the smallness of the MFE and a lack of curvature lead to sizable error bars for the kinetic parameters and would certainly benefit from the application of higher magnetic fields. Fortunately, including the reasonable assumptions of the expected viscosity dependence of k_{ce}, its value can be extrapolated from lower to higher temperatures and the accuracy of the assignment of k_{bet} and k_{TS} also increased. We now discuss in detail the results obtained for the various rate parameters.

Rate Constant of Cage Escape. Throughout the literature the Eigen−Debye equation[52] is widely used for estimating the rate constant of separation of a pair of unbound particles, eventually taking into account the effect of Coulombic forces if the particles are charged. In general form, the Eigen−Debye equation is expressed as

$$k_{ce} = \frac{3D_{1,2}}{a^2}\frac{\exp(W(a)/kT)}{a\int_a^\infty r^{-2}\exp(W(r)/kT)\,dr} \tag{23}$$

where $D_{1,2}$ is the relative diffusion coefficient of the two particles, a the reaction distance, and $W(r)$ the work needed to bring the particles from infinity to the distance r. According to the Stokes−Einstein equation, the relative diffusion coefficient $D_{1,2}$ of the two particles is inversely proportional to the viscosity η of the solvent:

$$D_{1,2} = \frac{kT}{6\pi\eta}\left(\frac{1}{r_1}+\frac{1}{r_2}\right) \tag{24}$$

Here r_1 and r_2 are the individual radii of the two particles. Combining eqs 23 and 24, the constant A in eq 14 can be expressed as

$$A = \frac{kT}{2\pi a^2}\left(\frac{1}{r_1}+\frac{1}{r_2}\right)\frac{\exp(W(a)/kT)}{a\int_a^\infty r^{-2}\exp(W(r)/kT)\,dr} \tag{25}$$

From a least-squares fit of our k_{ce} data from the MFE simulations, a value of $A = 2.0 \times 10^9$ s^{-1} has been obtained. Theoretically, A should be proportional to the temperature T. However, the deviations from the central temperature amount to only ± 16%, which will be neglected in our discussion. The theoretical value of A for 25 °C according to eq 25 is 5.4×10^9 s^{-1} if the extended Debye−Hückel expression for $W(r)$, e.g., given in ref 30, is used. Thus the values of k_{ce} determined from the magnetic field dependence of φ_{ce} is about 2.8 times smaller than predicted by the Eigen−Debye equation. When discussing this discrepancy, one should keep in mind that a geminate reaction of freely diffusing particles should be properly described with continuous diffusion theory. Actually the diffusional description cannot be unambiguously reduced to a reaction model employing first-order rate processes only (see ref 19 and references given therein). The Eigen−Debye assignment of k_{ce} is derived by combining the rate constant of a bimolecular

diffusion-controlled reaction with the equilibrium constant of contact pair formation between the two particles. The expression employed for the equilibrium constant contains some arbitrariness with regard to the interval of distances that is admissible to define a contact pair. It is noteworthy that, by employing diffusion dependent theory for general, not necessarily diffusion-controlled reactions, Kikuchi and co-workers[58] using Tachiya's method[59] arrived at a value of k_{ce} that is only 1/3 of the value from the Eigen−Debye equation. Thus, their result would be very close to what we find from our k_{ce} data. Finally, in our laboratory magnetic field effects on φ_{ce} have been simulated using a SLE based on the continuous diffusion equation. Reanalyzing the $\varphi_{ce}(B_0)$ curves simulated in this way for various values of $D_{1,2}$ in terms of the three-rate-constant model as employed for the analysis of our experimental $\varphi_{ce}(B_0)$ data in this paper, the dependence of k_{ce} on $D_{1,2}$ was 2 times smaller than predicted from the Eigen−Debye equation.[32,60] Thus there is good evidence that the k_{ce} values determined by fitting our experimental data with curves based on the SLE for the exponential model are reasonable and reliable.

Electron Spin Relaxation Time. The parameter τ_S has been obtained by two completely different methods: NMR of the $Ru(bpy)_3^{3+}$ complex and MFE in the photoreaction between $*Ru(bpy)_3^{2+}$ and MV^{2+}. In the overlapping temperature range of the results from the two methods, the τ_S values differ by less than 25%. Exactly equal values of 17.5 ps are obtained with both methods at ∼30 °C. In view of the different methods employed, this is an excellent agreement. The activation energies resulting from the Arrhenius plots of the τ_S values from the two methods differ by about a factor of 2. At present it is not clear whether this is a systematic deviation due to the different methods or the different solvents. The τ_S data from the MFE in aqueous solution exhibit a small "jump" around 30 °C.

The spin relaxation times observed are clearly shorter than the orientational relaxation times τ_R that may be estimated from the Debye relation[61]

$$\tau_R = \frac{\frac{4}{3}\pi r^3 \eta}{kT} \tag{26}$$

where r is the radius of the molecule and η the solvent viscosity. By using $r = 7$ Å for the $Ru(bpy)_3^{3+}$ complex, we obtain τ_R values between 567 and 124 ps in the temperature range from 5 °C to 69 °C, whereas the values of τ_S range from 30 to 12.5 ps. From this comparison it follows that the mechanism of spin relaxation cannot be related to molecular rotation. A similar conclusion has been arrived at by Doddrell and co-workers who suggested that a dynamic Jahn−Teller effect[62] or a vibronic Orbach mechanism[63] might be responsible. From our results there is rather convincing evidence that τ_S is field independent. Nuclear spin relaxation times measured for $[Ru(acac)_3]^{3+}$ at different magnetic fields[64] lend further support to this assumption. It should be noted that field-independent relaxation is a strong indication of the Orbach mechanism, where thermal population of higher electronic or vibronic Kramers doublets is the essential principle. Such a mechanism would also imply that $\tau_S = T_1 = T_2$, as has been assumed in our analysis.

Rate Constant of Backward Electron Transfer. Since k_{ce} and τ_S are reliable from comparison with data from independent sources, the consistency of our analysis strongly suggests that the k_{bet} values based on the MFE should be reliable too.[65] The values found for k_{bet} (i.e., for the fully spin-allowed backward electron transfer) in the present system range between 10 and 20 ps and show only a weak temperature dependence (E_a = 9.1 kJ mol^{-1} $\hat{=}$ 760 cm^{-1}). The observed values represent a very fast electron transfer process. This is consistent with the expectation that with $\Delta G^{\theta}_{bet} = -1.7$ eV[43] the system should be near the top of the Marcus curve in the Marcus inverted region.

5. Conclusion

In this work we have shown that the study of the magnetic field dependence of the cage escape efficiency in radical pairs involving strongly spin−orbit coupled systems such as the $[Ru(bpy)_3]^{3+}$ complex yields a complete quantitative picture of the diffusional, spin, and reaction processes competing in such systems. The accuracy at which the various rate constants on the picosecond time scale can be determined without further assumptions has been assessed. In systems where the photoinduced forward electron transfer is slower than backward electron transfer (either because it is intermolecular and limited by the quencher concentration or because of insufficient thermodynamic driving force, e.g., in intramolecular electron transfer of supramolecular compounds (see, e.g., ref 17)), the MFE based method is the only one to resolve k_{bet}. Furthermore, effective backward electron transfer rate constants observed for radical pairs involving strongly spin−orbit coupled paramagnetic metal complexes by direct time-resolved methods should be treated with caution, since spin processes might dominate the observed rates. The study of MFEs in strong magnetic fields provides a unique means to discriminate such kinetic contributions.

Acknowledgment. Support of this work by the priority program "Intra- and Intermolecular Electron Transfer" of the Volkswagenstiftung is gratefully acknowledged.

References and Notes

(1) Lepley, A. R.; Closs, G. L. *Chemically Induced Magnetic Polarization*; Wiley: New York, 1973.

(2) *Chemically induced magnetic polarization : proceedings of the NATO Advanced Study Institute*; Sogesta, Urbino, Italy, April 17−30, 1977; Muus, L. T., Atkins, P. W., McLauchlan, K. A., Pedersen, J. B., Eds.; Reidel: Dordrecht, 1977.

(3) Salikhov, K. M.; Molin, Yu. N.; Sagdeev, R. Z.; Buchachenko, A. L. *Spin Polarization and Magnetic Effects in Radical Reactions* Elsevier: Amsterdam, 1984.

(4) Nagakura S.; Hayashi H.; Azumi T. *Dynamic Spin Chemistry*; Kodansha: Tokyo, 1998.

(5) Steiner, U. E.; Ulrich, T. *Chem. Rev.* **1989**, *89*, 51.

(6) Steiner, U. E.; Wolff, H.-J. Magnetic Field Effects in Photochemistry in *Photochemistry and Photophysics*; Rabek, J. J., Scott, G. W., Eds.; CRC Press: Boca Raton, 1991; Vol. IV, p 1.

(7) Banci, L.; Bertini, I.; Luchinat, C. *Nuclear and electron relaxation*; VCH: Weinheim, 1991.

(8) Ferraudi, G.; Arguello, G. A. *J. Phys. Chem.* **1988**, *92*, 1846.

(9) Steiner, U. E.; Wolff, H.-J.; Ulrich, T.; Ohno, T. *J. Phys. Chem.* **1989**, *93*, 5147.

(10) Bürssner, D.; Wolff, H.-J.; Steiner, U. E. *Z. Physik. Chem. N. F.* **1993**, *182*, 297.

(11) Wolff, H.-J.; Steiner, U. E. *Z. Physik. Chem. N. F.* **1990**, *169*, 147.

(12) Bürssner, D.; Wolff, H.-J.; Steiner, U. E. *Angew. Chem., Int. Ed. Engl.* **1994**, *33*, 1772.

(13) Wolff, H.-J.; Bürssner, D.; Steiner, U. E. *Pure Appl. Chem.* **1995**, *67*, 167.

(14) Steiner, U. E.; Bürssner, D. *Z. Physik. Chem. N. F.* **1990**, *169*, 159.

(15) Krissinel, E. B.; Burshtein, A. I.; Lukzen, N. N.; Steiner, U. E. *Mol. Phys.* **1998**, *96*, 1083.

(16) Gilch, P.; Haas, W.; Steiner, U. E. *Chem. Phys. Lett.* **1996**, *254*, 384.

(17) Klumpp, T.; Linsenmann, M.; Bürssner, D.; Krissinel, E. B.; Larson, S. L.; Elliott, C. M.; Steiner, U. E. *J. Am. Chem. Soc.* **1999**, *121*, 1076.
(18) Gorelik, E. V.; Lukzen, N. N.; Sagdeev, R. Z.; Steiner, U. E. *Chem. Phys.* **2000**, *262*, 303.
(19) Burshtein, A. I.; Krissinel, E.; Steiner, U. E. *Phys. Chem. Chem. Phys.* **2001**, *3*, 198.
(20) Gilch, P.; Pöllinger-Dammer, F.; Steiner, U. E.; Michel-Beyerle, M. E. *Science* **1998**, *281*, 982.
(21) Mukai, M.; Tanaka, H.; Fujiwara, Y.; Tanimoto, Y. *Bull. Chem. Soc. Jpn.* **1994**, *67*, 3112.
(22) Ferraudi, G. *J. Phys. Chem.* **1993**, *97*, 11929.
(23) Ferraudi, G. *Chem. Phys. Lett.* **1993**, *203*, 487.
(24) Ferraudi, G. *J. Phys. Chem.* **1993**, *97*, 2793.
(25) Ronco, S.; Perkovic, M.; Ferraudi, G.; Cozzi, M. *Chem. Phys.* **1992**, *162*, 95.
(26) Ronco, S.; Ferraudi, G. *Inorg. Chem.* **1990**, *29*, 3961.
(27) Ronco, S.; Ferraudi, G. *J. Chem. Soc., Dalton Trans.* **1990**, 887.
(28) Hoffman, M. Z. *J. Phys. Chem.* **1988**, *92*, 3458.
(29) Hoffman, M. Z. *J. Phys. Chem.* **1991**, *95*, 2606.
(30) Clark, C. D.; Hoffman, M. Z. *J. Phys. Chem.* **1996**, *100*, 7526.
(31) Furrer, G. Diploma Thesis, University of Fribourg, 1987.
(32) Linsenmann, M. Doctoral Dissertation, University of Konstanz, 1997.
(33) Orellana, G.; Braun, A. M. *J. Photochem. Photobiol. A: Chem.* **1989**, *48*, 277.
(34) Nozaki, K.; Linsenmann, M.; Ohno, T. in ref 32.
(35) Krissinel, E. B.; Steiner, U. E. *QYIELD*, computer program for calculating the quantum yield and magnetic field effect of radical separation in liquid-phase reactions, Konstanz, 1999. The program is available on request.
(36) Burshtein, A. I.; Krissinel, E. B.; Mikhelashvili, M. S. *J. Phys. Chem.* **1994**, *98*, 7319.
(37) Krissinel, E. B.; Agmon, N. *J. Comput. Chem.* **1996**, *17*, 1085.
(38) This term has been coined in consideration of the exponential decay function it predicts for the RPs as a consequence of the first-order kinetic description.[3] It should not be confused with the exponential distance law for $k_{bet}(r)$ used in the diffusional model.
(39) Dennis, J. E.; Shnabel, R. B. *Numerical Methods for Unconstrained Optimization and Nonlinear Equations*; Prentice-Hall: Englewood Cliffs, NJ, 1983.
(40) DeSimone, R. E.; Drago, R. S. *J. Am. Chem. Soc.* **1970**, *92*, 2343.
(41) La Mar, G. N.; Horrocks, W. D.; Holm R. H. *NMR of paramagnetic molecules*; Academic Press: New York, 1973.
(42) Solomon, I. *Phys. Rev.* **1955**, *99*, 559.
(43) Wolff, H.-J. Doctoral Dissertation, University of Konstanz, 1994.
(44) Bertini, I.; Luchinat, C.; Vasavada, K. V. *J. Magn. Reson.* **1990**, *89*, 243.
(45) Vasavada, K. V.; Rao, B. D. N. *J. Magn. Reson.* **1989**, *81*, 275.
(46) Biner, M.; Bürgi, H.-B.; Ludi, A.; Röhr, C. *J. Am. Chem. Soc.* **1992**, *114*, 5197.
(47) According to the Debye equation $\tau_r = 4\pi\eta b^3/(3kT)$where η is the solvent viscosity and b the radius of a molecule. For example, for 40 °C where the viscosity η of CH_3CN/H_2SO_4 (9: 1, v/v) is 0.66 cP, a value of 430 ps for is obtained for τ_R when using $b = 7$ Å.
(48) Unfortunately there are a few sign misprints in equations (10) of ref 14. The correct equations read:

$$T'_+ \equiv |\alpha\alpha'\rangle = \sin(x)T_+(a_1r) + \frac{1}{\sqrt{2}}\cos(x)[T_0(e_-r) - S(e_-r)]$$

$$T'_- \equiv |\beta\beta'\rangle = \sin(x)T_-(a_1r) + \frac{1}{\sqrt{2}}\cos(x)[T_0(e_+r) + S(e_+r)]$$

$$T'_0 \equiv \frac{1}{\sqrt{2}}(|\alpha'\beta\rangle + |\beta'\alpha\rangle) = \sin(x)T_0(a_1r) + \frac{1}{\sqrt{2}}\cos(x)[T_+(e_+r) + T_-(e_-r)]$$

$$S' \equiv \frac{1}{\sqrt{2}}(|\alpha'\beta\rangle - |\beta'\alpha\rangle) = \sin(x)S(a_1r) - \frac{1}{\sqrt{2}}\cos(x)[T_+(e_+r) - T_-(e_-r)]$$

(49) Bürssner, D. Diploma Thesis, University of Konstanz, 1989.
(50) To determine the standard errors of any of these parameters we calculated expressions of the following type, e.g., in case of the parameter τ_S:

$$\overline{d\tau_S^2} = \frac{1}{N}\sum_{i=1}^{N}(\varphi_{ce,i} - \varphi_{ce,i}^{calc})^2\sum_{k=1}^{N}\left(\frac{\partial\tau_S}{\partial\varphi_{ce,k}}\right)^2_{\varphi_{ce,l\neq k}}$$

The partial differential quotient $(\partial\tau_S/\partial\varphi_{ce,k})_{\varphi_{ce,l\neq k}}$ was estimated as a quotient of differences $\Delta\tau_S/\Delta\varphi_{ce,i}$ obtained by shifting φ_{ce} of the kth data point by a small increment $\Delta\varphi_{ce}$ and recalculating the best fit yielding the shifts of the fit parameters $\Delta\tau_S$, Δk_{ce}, Δk_{bet}.
(51) Clark, C. D.; Hoffman, M. Z. *J. Phys. Chem.* **1996**, *100*, 14688.
(52) Eigen, M. *Z. Physik. Chem. N. F.* **1954**, *1*, 176.
(53) The absolute values of k_{bet} in ref 54 are actually larger by a factor of 2.5−3 because a larger value of k_{ce} (from the Eigen−Debye equation) was used (see discussion of k_{ce}).
(54) Supporting Information available to ref 30.
(55) For a ps-time-resolved observation of the magnetic modulation of an electron-transfer reaction, see ref 20.
(56) Due to the spin−orbit-coupling properties of the complex, Δg is strongly anisotropic and $\Delta\omega_L$ depends on the orientation of the complex in the magnetic field. In the theoretical simulation the effects of $\Delta\omega_L$ have to be averaged over an isotropic orientational distribution.
(57) The theoretical model predicts that the MFE should be saturated at high magnetic fields of some 10 T. Thus the initial slope and the limiting value of the MFE would be important characteristic observables. If the saturation limit cannot be reached, the curvature at low fields still carries information that allows reliable extrapolation to the saturation limit (depending on the degree of saturation actually reached).
(58) Niwa, T.; Kikuchi, K.; Matsusita, N.; Hayashi, M.; Katagiri, T.; Takahashi, Y.; Miyashi, T. *J. Phys. Chem.* **1993**, *97*, 11960.
(59) Sano, H.; Tachiya, M. *J. Chem. Phys.* **1979**, *71*, 1276.
(60) These calculations also provide evidence that in the range of $D_{1,2}$ values scanned in the course of temperature variation in this work, we are definitely in the range where the "exponential" model is reasonable enough. The criterion is that the values of k_{bet} evaluated from MFE curves corresponding to different $D_{1,2}$ values (other parameters being constant) should be independent of the $D_{1,2}$ values.[19,32]
(61) Debye, P. *Polar Molecules*; Dover Publications: New York, 1945.
(62) Doddrell, D. M.; Bendall, M. R.; Pegg, D. T.; Healy, P. C. *J. Am. Chem. Soc.* **1977**, *99*, 1281.
(63) Kleinschmidt, K. M.; Dobson, J. F.; Doddrell, D. M. *Chem. Phys. Lett.* **1979**, *68*, 115.
(64) Doddrell, D. M.; Pegg, D. T.; Bendall, M. R.; Gregson, A. K. *Aust. J. Chem.* **1977**, *30*, 1635.
(65) For the ferrocenium$^+$/(methylene blue)$^\bullet$ system, a value of 1.5 ps was derived for the time constant of backward electron transfer.[16] In fact, direct time-resolved observations in similar systems (*N*,*N*-dimethylamino-ferrocenium$^+$/(methylene blue)$^\bullet$ 1 ps,[66] ethylferrocenium$^+$/oxonine$^\bullet$, 0.6 ps[20]) yielded reaction time constants close to that value.
(66) Gilch, P.; Pöllinger-Dammer, F.; Steiner, U. E.; Michel-Beyerle, M. E. *Chem. Phys. Lett.* **1997**, *275*, 339.